

Time–temperature–property curves for quench sensitivity of 6063 aluminum alloy

Hong-ying LI^{1,2}, Cui-ting ZENG¹, Mao-sheng HAN¹, Jiao-jiao LIU¹, Xiao-chao LU¹

1. School of Materials Science and Engineering, Central South University, Changsha 410083, China;

2. Key Lab of Nonferrous Materials, Ministry of Education, Central South University, Changsha 410083, China

Received 12 Mach 2012; accepted 12 June 2012

Abstract: The quench sensitivity of 6063 alloy was investigated via constructing time–temperature–property (TTP) curves by interrupted quenching technique and transmission electron microscopy (TEM) analysis. The results show that the quench sensitivity of 6063 alloy is lower than that of 6061 or 6082 alloy, and the critical temperature ranges from 300 to 410 °C with the nose temperature of about 360 °C. From TEM analysis, heterogeneous precipitate β -Mg₂Si is prior to nucleate on the (Al_xFe_ySi_z) dispersoids in the critical temperature range, and grows up most rapidly at the nose temperature of 360 °C. The heterogeneous precipitation leads to a low concentration of solute, which consequently reduces the amount of the strengthening phase β'' after aging. In the large-scale industrial production of 6063 alloy, the cooling rate during quenching should be enhanced as high as possible in the quenching sensitive temperature range (410–300 °C) to suppress the heterogeneous precipitation to get optimal mechanical properties, and it should be slowed down properly from the solution temperature to 410 °C and below 300 °C to reduce the residual stress.

Key words: 6063 aluminum alloy; quench sensitivity; hardness; time–temperature–property curve; strengthening phase; heterogeneous precipitation; residual stress

1 Introduction

6063 alloy is widely used for the application of construction and transportation due to its attractive combination of mechanical properties, processability and stress corrosion resistance [1,2]. As a kind of precipitation-hardened aluminum alloy, the high strength of 6063 alloy is mainly obtained via the formation of fine precipitates originated from the decomposition of super-saturated solid solution. Many surveys have focused on the fine precipitates, which were generally developed by homogeneous nucleation during artificial aging [3,4]. However, quenching is also one of the most critical factors to affect the aging hardening effect of 6063 alloy. Theoretically, the quenching for Al–Mg–Si alloys should be done as quickly as possible to suppress the decomposition of solid solution [5,6]. Nevertheless, it is necessary for large-scale production to cool at an appropriately slow rate to reduce the residual stress and distortion. The alloy with a potential high strength would get low mechanical property if it is cooled too slowly [7,8]. And during this process, heterogeneous

precipitation would appear and have negative effects on the final mechanical properties [9]. The quantity of the heterogeneous precipitates is critical with respect to the final mechanical properties such as hardness, yield stress and toughness [10]. Since different alloy has different sensitivity regarding the quenching rate, it is significant to control the quenching process through the investigations for quench sensitivity of 6063 alloy. The quench sensitivity can be studied by TTP curves, which are the loci of the incubation period and identify the time required to attain some fraction of the required property at a set transformation temperature [11,12].

The approach of interrupted quenching technique was first used by FINK and WILLEY [11] to construct the TTP curves of strength of 7075 alloy. Afterwards, plenty of work has been done on the TTP curves of Al–Zn–Mg–Cu alloys [13–16]. According to previous literatures, the TTP curves for some typical Al–Mg–Si alloys, such as 6061 and 6082, could be available [13,17]. However, few studies on exploring the TTP curves of 6063 alloy were reported in the scientific literatures.

In this work, in order to investigate the quench sensitivity of 6063 alloy, the TTP curves of 6063 alloy

were determined by interrupted quenching technique, and the important constants k_2 – k_5 and the critical temperature range for 6063 alloy were identified. Moreover, the morphologies of heterogeneous precipitation were also analyzed by the transmission electron microscopy (TEM).

2 Experimental

The chemical composition (mass fraction, %) of hot-extruded 6063 alloy used in the present work was Al–0.35Si–0.60Mg–0.10Fe–0.01Cu.

20 mm(L)×20 mm(ST)×10 mm(LT) mm specimens were used to determine the TTP curves. After solution heat treatment at 535 °C for 1 h, samples were transferred rapidly (<3 s) to a salt bath containing 50% sodium nitrite and 50% potassium nitrate eutectic mixture, and then held isothermally for set periods of time. The selected isothermal temperatures ranging from 230 to 460 °C, the salt temperature was constantly monitored and maintained at ±3 °C of the required temperature for the duration of the isothermal holding. The specimens were quenched into room temperature (<20 °C) water after the specimens were held at the isothermal temperature for the desired time. Samples were finally aged at 180 °C for 4 h and then measured by Brinell hardometer to create the TTP curves.

Hardness measurement was performed on a HBE–3000 Brinell hardometer with a load of 2.452 kN and an indentation time of 30 s. The TEM examination was carried out in a TECNAIG² 20 instrument, operated at 200 kV. Specimens for TEM examination were cut from various states under different heat treatment conditions with an electrical-discharge machine. Thin foils were mechanically ground to used discs with about 80 μm in thickness and 3 mm in diameter. Then a twin-jet electropolisher was used to produce electron-transparent thin sections in these slice discs with a solution of 30% nitric acid and 70% methanol at –30 °C. Additionally, the energy-dispersive X-ray (EDX) experiments were preformed on the selected micro zones.

3 Results and discussion

3.1 TTP curves

After the sample was thermally treated at 535 °C for 1 h, then quenched to room temperature (<20 °C) and aged at 180 °C for 4 h, its Brinell hardness is HB84, which is defined as the maximum property. Figure 1 represents the influence of isothermal treatment on the hardness of aged specimens. It can be found that the hardness of the studied alloy tends to decrease overall with the extension of isothermal time, and the decreasing rate is correlated to the isothermal temperature. When

held at 370 °C, the hardness decreases sharply from the maximum hardness HB84 to HB39.3 within 500 s, dropping by 53.2%, and then roughly maintains stable. While at lower temperature, the hardness at 230 °C reduces from the maximum hardness HB84 to HB76 within 1000 s, dropping by 9.5%. At a higher temperature, the hardness at 460 °C declines at a much lower rate from the maximum value HB84 to HB80.7 within 1000 s, only dropping by 4%.

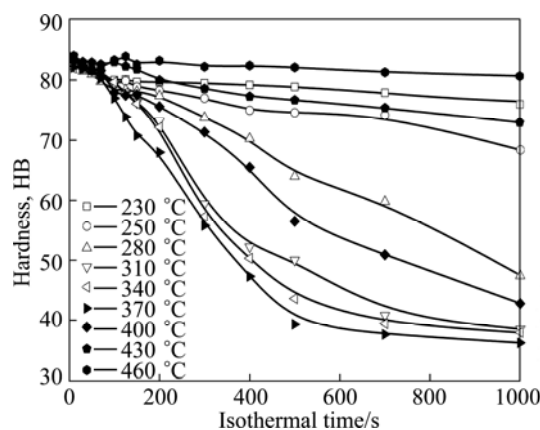


Fig. 1 Influence of holding time at different temperatures on hardness of Al–0.35Si–0.60Mg–0.10Fe–0.01Cu after artificial aging

TTP curve is an effective approach to evaluate the quench sensitivity. It is generally accepted that the TTP curves can be described mathematically as $C_t(T)$ shown in Eq. (1)[18].

$$C_t(T) = -k_1 k_2 \exp \left[\frac{k_3 k_4^2}{RT(k_4 - T)^2} \right] \exp \left(\frac{k_5}{RT} \right) \quad (1)$$

where $C_t(T)$ is the critical time required to precipitate a constant amount of solute; k_1 is the constant equal to the natural logarithm of the fraction untransformed during quenching; k_2 is the constant related to the reciprocal of the number of nucleation sites; k_3 is the constant related to the energy required to form a nucleus; k_4 is the constant related to the solvus temperature; k_5 is the constant related to the activation energy for diffusion; R is the mole gas constant; T is the thermodynamic temperature.

$C_t(T)$ function can be used to determine the incubation time for the studied alloy. According to its hardness data, the time to achieve 90% of the maximum hardness was determined and used to construct the TTP curve. The coefficients in the above equation were evaluated by the iterative non-linear fitting method. The resultant 90% TTP curve and the determined k_2 – k_5 coefficients are shown in Fig. 2 and Table 1, respectively. And the k_2 – k_5 constants enable the minimum misfit between the fitted and measured hardness values.

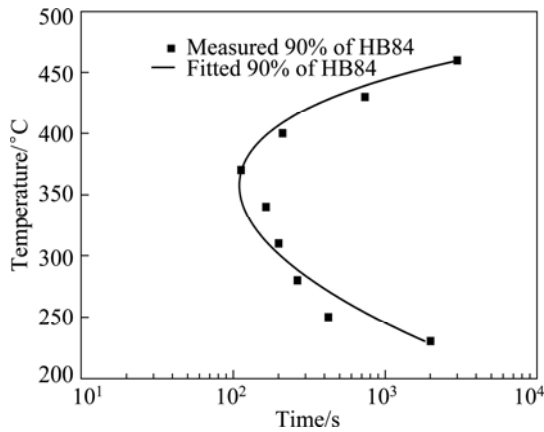


Fig. 2 TTP curve for 90% of the maximum property by measurement and fitting

Table 1 Coefficients of TTP curve equation for studied alloy by fitting

| k_2/s | $k_3/(J \cdot mol^{-1})$ | k_4/K | $k_5/(J \cdot mol^{-1})$ |
|-----------------------|--------------------------|---------|--------------------------|
| 4.8×10^{-10} | 4146 | 946 | 111627 |

The values in Table 1 were substituted in $C_i(T)$ function (Eq. (1)) and TTP curves of 80%, 90%, 95% and 99.5% of the maximum property were constructed via changing the constant k_1 , as shown in Fig. 3. According to the location of the TTP curve for 99.5% of the maximum property, when the transformation time is 10 s, the critical temperature range is determined between approximately 300 °C and 410 °C, and the nose temperature of TTP curves is about 360 °C. In this critical temperature range, the hardness decreases rapidly with the extension of isothermal time, but when the isothermal temperature is lower than 300 °C or higher than 410 °C, the hardness decreases much slower as the isothermal time extends.

Table 2 Critical temperature range and nose temperature with critical time of TTP curves for some typical Al–Mg–Si alloys [13,17]

| Alloy | Critical temperature range/°C | Nose temperature/°C | Critical time/s |
|------------|-------------------------------|---------------------|-----------------|
| 6063 alloy | 300–410 | 360 | 5 |
| 6061 alloy | 220–440 | 360 | 0.8 |
| 6082 alloy | 250–440 | 360 | 1.2 |

As shown in Fig. 3, when the hardness falls about 0.5% at the nose temperature of the studied alloy, the critical time is 5 s. The critical temperature range and nose temperature with the critical time of TTP curves for 6061 and 6082 alloys from literatures are indicated in Table 2 [13,17]. As can be seen, these alloys have same

nose temperature, but differ in critical time and temperature zone. The 6061 alloy has the largest critical temperature of 220 °C, while the studied alloy has the smallest temperature of 110 °C. The shortest critical time of about 0.8 s is observed for 6061 alloy, while the longest critical time is about 5 s for the studied alloy. According to the above studies, 6061 alloy has the highest quench sensitivity while the studied alloy has the lowest quench sensitivity.

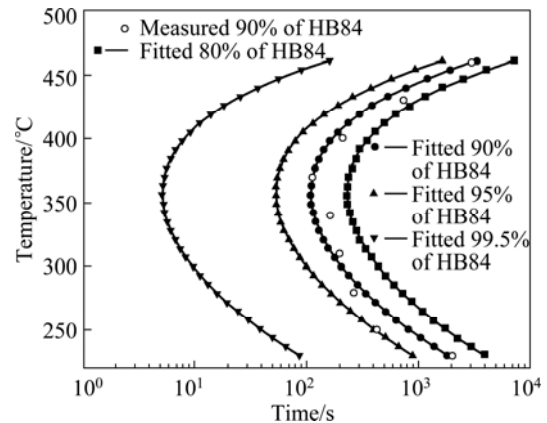


Fig. 3 TTP curves of studied alloy

3.2 TEM observation and EDX analysis

According to the TTP curves of the studied alloy, TEM and EDX were applied to investigating the evolution of the heterogeneous precipitation held at 360 °C. The morphologies held at 290 °C and 420 °C for 10 s were also investigated.

Figure 4 shows the bright-field TEM images of the studied alloy held at 290 °C and 420 °C, respectively, for 10 s. It can be seen that the matrices of the two conditions are very pure without any precipitates, which indicates that the alloy is still in the incubation periods during the isothermal treatments of both 290 °C and 420 °C for 10 s.

Figure 5 shows the microstructures of quenched specimens held at 360 °C. With regard to the sample treated for 10 s which is a little longer than the critical time required to precipitate 0.5% solute, there are no coarse precipitates in the matrix but a few granular dispersed particles (arrow) as shown in Fig. 5(a). To the sample treated for 120 s which is the critical time required to precipitate 10% solute, there are some coarse β -Mg₂Si equilibrium precipitates with a length of 0.5–1 μ m in the matrix, as shown in Fig. 5(b). With regard to the sample treated for 250 s, which is the critical time required to precipitate 20% solute, both of the density and the size of coarse equilibrium β -Mg₂Si precipitates are increased remarkably as shown in Fig. 5(c). With regard to the sample treated for 1000 s, the coarse equilibrium β -Mg₂Si phase precipitates have further grown up as shown in Fig. 5(d).

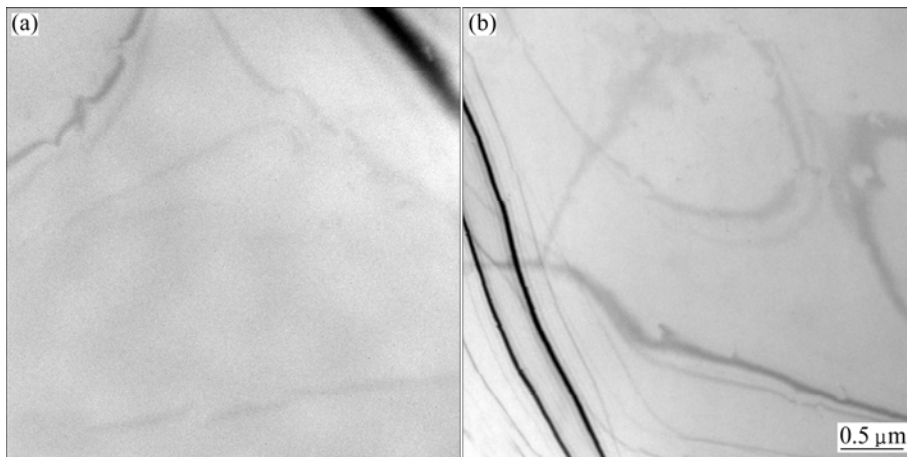


Fig. 4 TEM images of quenched specimens held at 290 °C (a) and 420 °C (b) for 10 s

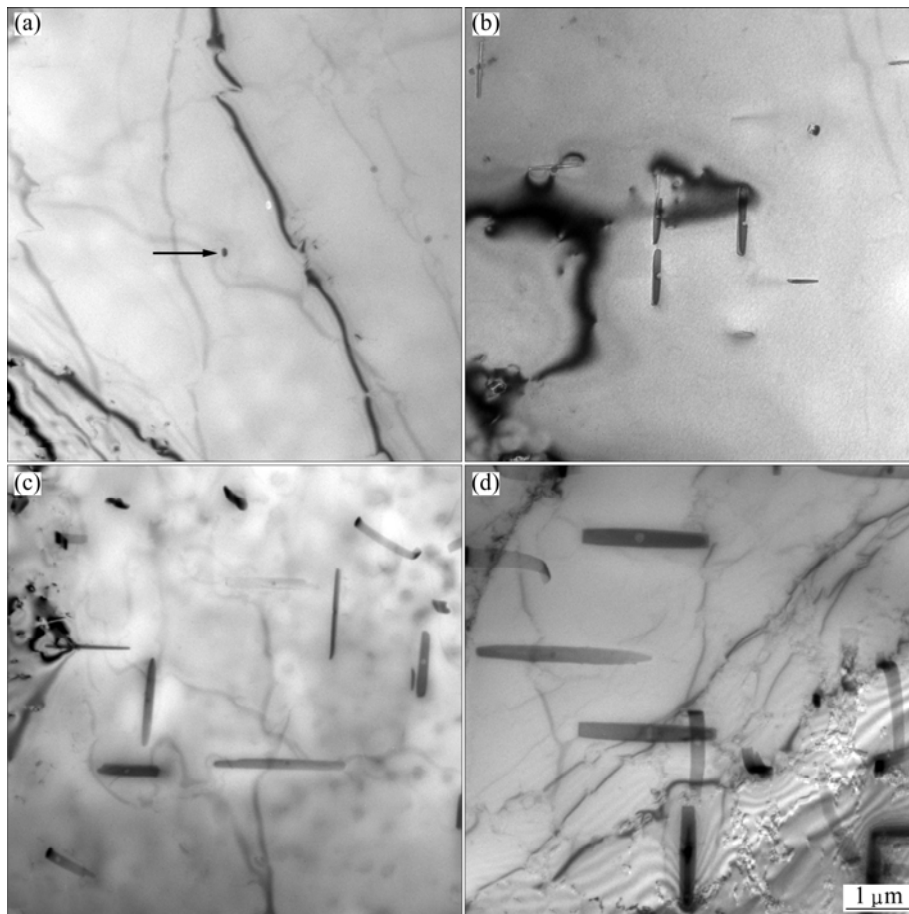


Fig. 5 TEM images of quenched specimens held at 360 °C for 10 s (a), 120 s (b), 250 s (c) and 1000 s (d)

Generally, the quench sensitivity increases with the concentration of alloying elements and the density of nucleation sites for the precipitates [14]. Figures 6(a), (b) and (c) show images of the intragranular heterogeneous β precipitates under higher magnification. It can be seen that each rod-shaped β precipitate nucleates on a smaller sphere particle. EDX analysis was applied to these sphere particles and the resulted spectra were shown in Figs. 6(a'), (b'), (c'). All spectra are dominated by the

characteristic X-ray signals of Al K_{α} , Si K_{α} and Fe K_{α} with only a small contribution from Mg K_{α} . This it clearly suggests that the preferred intragranular nucleation sites of the heterogeneous precipitates are $Al_xFe_ySi_z$ dispersoids in the studied alloy. Since the concentrations of Si and Fe for the studied alloy are lower compared with 6061 or 6082 alloy [13,17], the quantity of $(Al_xFe_ySi_z)$ dispersoids is not so sufficient, leading to lower quench sensitivity of the studied alloy

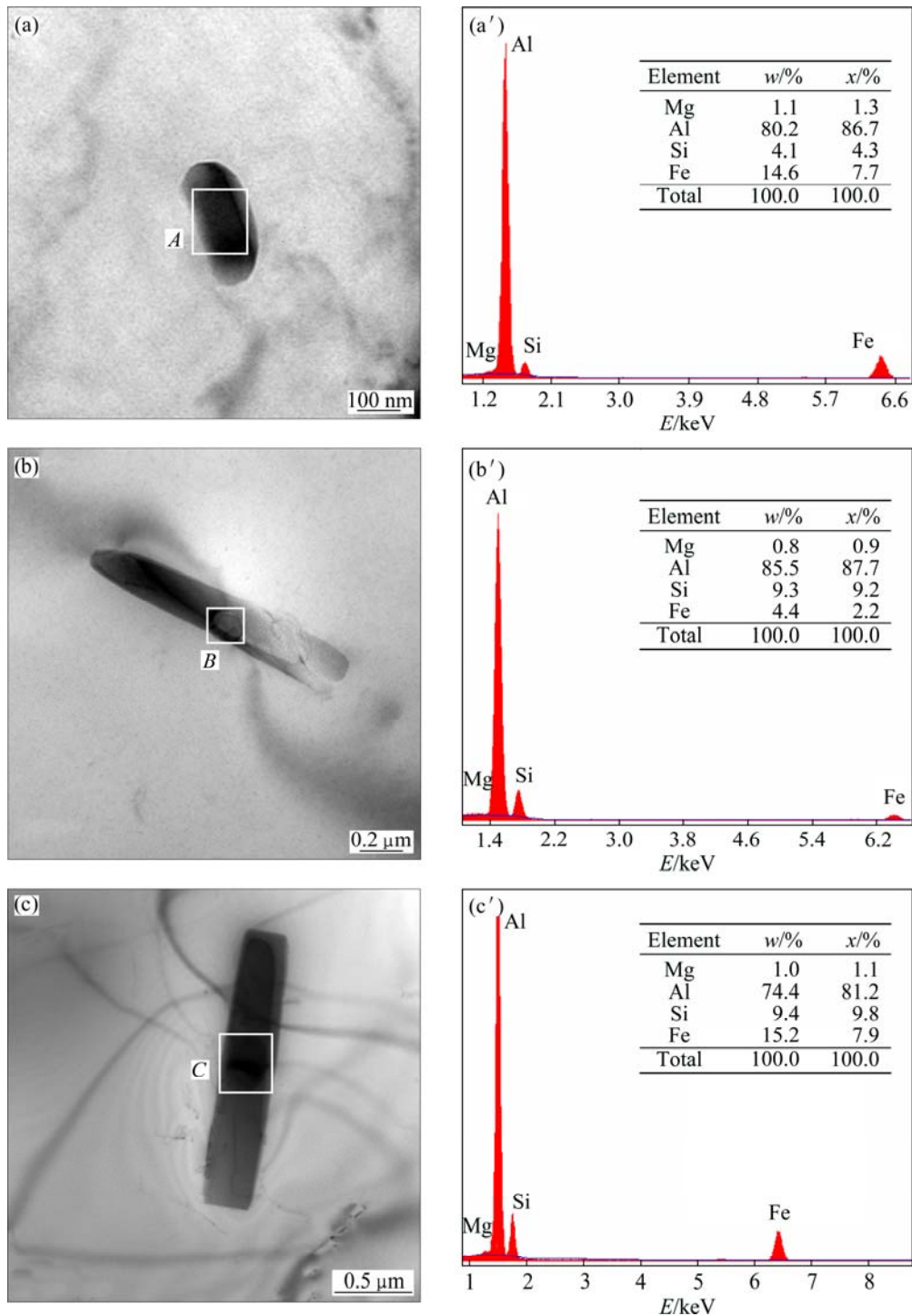


Fig. 6 TEM images of β precipitates held at 360 °C for (a) 10 s, (b) 250 s and (c) 1000 s and EDX spectra at position A (a'), B (b') and C (c')

than 6061 or 6082 alloys.

Figure 7 shows the mean size of the intragranular heterogeneous β precipitates developed at 360 °C (measured on TEM micrographs) and the hardness after quenching with extension of holding time. It can be found that the size of the heterogeneous β precipitates increases as well as the hardness decreases with the extension of isothermal holding time. During the

isothermal treatment, the decomposition of solid solution leads to the precipitation of equilibrium β -Mg₂Si phase. And the coarse β -Mg₂Si phase contributes little to the strength of the studied alloy as this precipitate is incoherent with the Al matrix. Furthermore, the effect of solid solution strengthening is weakened with the precipitation of equilibrium β -Mg₂Si phase, leading to a lower hardness after quenching. What is worse, the

precipitation of β -Mg₂Si phase leads to a lower concentration of solute elements, and inhibits the precipitate of strengthening phase β'' in artificial aging, which is proved by the following TEM observations as shown in Fig. 8.

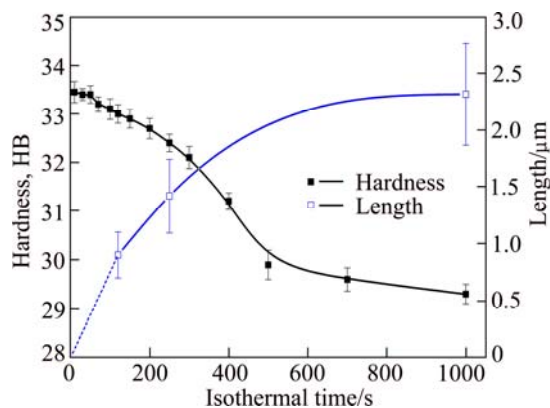


Fig. 7 Evolution of hardness with holding time at 360 °C and mean length of intragranular heterogeneous precipitates after quenching

Figure 8 shows the microstructures of the aged specimens held at 370 °C for different time. With the corresponding SAD patterns, it can be seen that the incident beam is parallel to a $\langle 100 \rangle$ zone axis of the Al matrix. As shown in Fig. 8(a), the specimen without isothermal holding contains a high density of fine homogeneous needle-shaped precipitates of 20–50 nm in length lying along the $\langle 100 \rangle$ directions of the matrix. For 10 s of isothermal treatment, two kinds of precipitates are observed lying along the $\langle 100 \rangle$ direction zone of the matrix shown in Fig. 8(b). One is needle-shaped precipitates with 20–50 nm in length, and the density of needle-shaped precipitates is reduced remarkably. And the other is rod-shaped precipitates with approximately 100 nm in length. It can be supposed that the rod-shaped precipitates have been formed during the isothermal holding process, and then continued to grow via the absorption of solute around them during artificial aging. As shown in Fig. 8(c), only coarse rod-shaped precipitates of 2–3 μm in length can be observed as the isothermal time reaches up to 1000 s, without any fine needle-shaped precipitates. The results demonstrate that most of the solute elements have been transformed into equilibrium β -Mg₂Si phase when the isothermal holding time is prolonged to 1000 s.

It is well known that the precipitation sequence of Al–Mg–Si alloys during aging can be expressed as super-saturated solid solution → atom clusters → G.P zone → needle-shaped β'' precipitate → rod-shaped β' precipitate → rod-shaped β -Mg₂Si [19,20]. Since G.P zone and β'' precipitate are completely or partially coherent with the matrix, and rod-shaped precipitates, especially rod-shaped β -Mg₂Si, have low coherency with

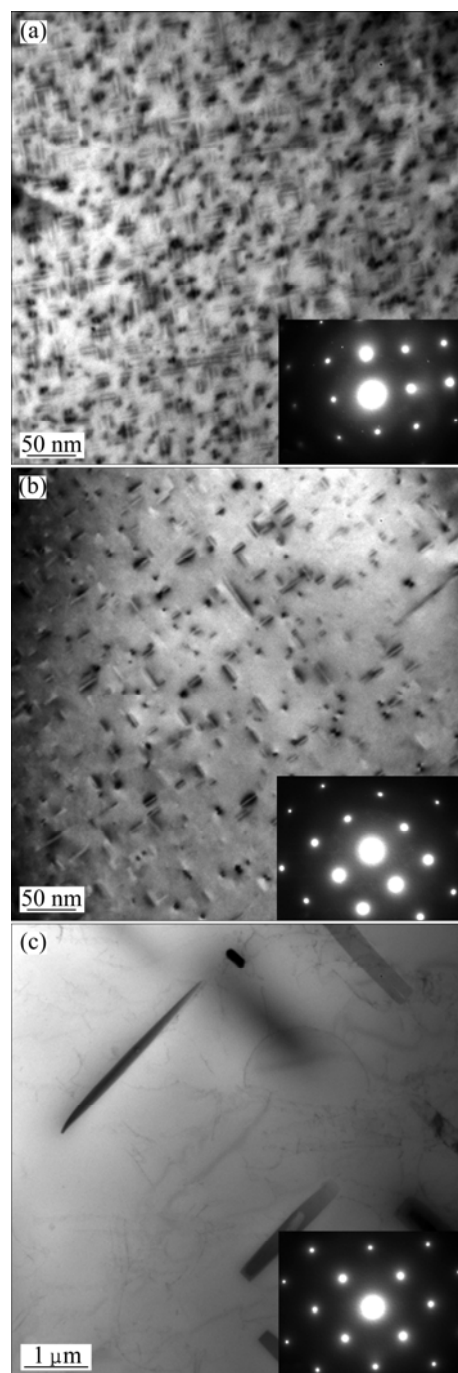


Fig. 8 TEM images of aged specimens held at 370 °C for 0 s (a), 10 s (b) and 1000 s (c)

the matrix [21–23], the mechanical properties of the studied alloy depend greatly on the density of G.P zone and needle-shaped β'' precipitate, but depend slightly on the density of rod-shaped β' and β precipitates. Figure 9 schematically summarizes the relationship between the precipitate distribution and the hardness of aged specimen when the isothermal temperature is 370 °C. As is shown, with the extension of holding time, the hardness after aging decreases sharply with more coarse particles formed, whereas the density of needle-shaped β'' precipitates reduces remarkably. For this phenomenon,

the equilibrium β -Mg₂Si precipitates, which nucleated on (Al_xFe_ySi_z) dispersoids and grew up during the isothermal holding treatment, have little hardening effect due to their large size and incoherent with the matrix. As a result of depleting of Mg and Si solute in the solid solution, less amount of hardening β'' precipitates could form after aging. Moreover, precipitates-free zones are created around these coarse precipitates. This kind of microstructure makes little contribution to the hardness after aging as shown in Fig. 9.

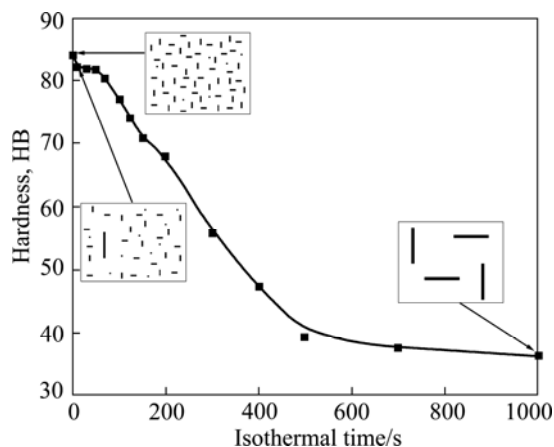


Fig. 9 Relationship between precipitate distribution and hardness of aged specimens held at 370 °C for different time

The solubility of Mg and Si in the Al matrix decreases with the reduction of temperature. Thus, a lot of equilibrium phases precipitate by heterogeneous nucleation in the supersaturated solution during the isothermal treatment. At temperatures above the nose of the curve but below the solvus temperature, long isothermal time is necessary for the precipitates to nucleate and grow up due to the low driving force available for transformation. When the temperature approaches the nose of the curve, the degree of supersaturation and the driving force available for precipitation increase, hence the time required for the precipitation reduces with the increasing of undercooling. Below the nose of the curve, the time required for precipitation increases again due to the low rate of solid-state diffusion.

According to the above discoveries, it can be found that when the cooling rate is too low during the continuous cooling after solution treatment, due to the growth of the coarse β -Mg₂Si phase, the degree of supersaturation of solid solution is reduced, resulting in the reduction of the follow-up aging strengthening effect. Moreover, the vacancy concentration becomes low due to the slow cooling rate, which may decrease the homogeneous nucleation rate during subsequent aging. When the cooling rate is adequate during the continuous cooling after solution treatment, the growth of the coarse

β -Mg₂Si phase can be restrained, resulting in high degree of supersaturation of the solid solution. Hence, the aging strengthening effect can be ensured. In order to obtain the greatest hardening effect in the subsequent aging, it is suggested that, in the large-scale industrial production of 6063 aluminum alloy, the cooling rate during quenching could be slowed down properly from the solution temperature to 410 °C; then it should be enhanced as high as possible in the quenching sensitive temperature range (410–300 °C); while below 300 °C, it should be slowed down again to get optimal mechanical properties.

4 Conclusions

1) The TTP curves have been constructed for 6063 alloy with the identification of important coefficients k_2 – k_5 . The critical temperature range is determined as 300–410 °C and the nose temperature is about 360 °C.

2) The β -Mg₂Si phase nucleates on the Al_xFe_ySi_z dispersoids heterogeneously and precipitates from the supersaturated solid solution of 6063 alloy within the critical temperature range, and the transformation occurs most rapidly at about 360 °C. The heterogeneous precipitation leads to a low concentration of solutes, and consequently reduces the amount of the strengthening phase β'' during aging, resulting in a lower hardness.

3) The quench sensitivity of 6063 alloy is lower than that of 6082 or 6061 alloy. It is suggested that, in the large-scale industrial production of 6063 alloy, the cooling rate during quenching should be slowed down properly from the solution temperature to 410 °C; then it should be enhanced as high as possible in the quenching sensitive temperature range (410–300 °C) to suppress the heterogeneous precipitation; while below 300 °C, it should be slowed down again to get optimal mechanical properties.

References

- [1] JI Yan-li, GUO Fu-an, PAN Yan-feng. Microstructural characteristics and paint-bake response of Al–Mg–Si–Cu alloy [J]. Transactions of Nonferrous Metals Society of China, 2008, 18(1): 126–131.
- [2] PANIGRAHI S K, JAYAGANTHAN R. A study on the mechanical properties of cryorolled Al–Mg–Si alloy [J]. Materials Science and Engineering A, 2008, 480(1–2): 299–305.
- [3] MARIOARA C D, ANDERSEN S J, JANSEN J, ZANDBERGEN H W. The influence of temperature and storage time at RT on nucleation of the β'' phase in a 6082 Al–Mg–Si alloy [J]. Acta Materialia, 2003, 51(3): 789–796.
- [4] CHEN Dong-chu, LI Wen-fang, GONG Wei-hui, WU Gui-xiang, WU Jian-feng. Microstructure and formation mechanism of Ce-based chemical conversion coating on 6063 Al alloy [J]. Transactions of Nonferrous Metals Society of China, 2009, 19(3): 592–600.
- [5] CAVAZOS J L, COLÁS R. Quench sensitivity of a heat treatable aluminum alloy [J]. Materials Science and Engineering A, 2003, 363(1): 171–178.

- [6] MILKEREIT B, WANDERKA N, SCHICK C, KESSLER O. Continuous cooling precipitation diagrams of Al–Mg–Si alloys [J]. *Materials Science and Engineering A*, 2012, 550: 87–96.
- [7] LI Song-ru, ZHOU Shan-chu. Heat treatment of metals [M]. Changsha: Central South University Press, 2005: 244–249. (in Chinese)
- [8] CAVAZOS J L, COLÁS R. Precipitation in a heat-treatable aluminum alloy cooled at different rates [J]. *Materials Characterization*, 2001, 47(3–4): 175–179.
- [9] EVANCHO J W, STALEY J T. Kinetics of precipitation in aluminum alloys during continuous cooling [J]. *Metallurgical and Materials Transactions B*, 1974, 5(1): 43–47.
- [10] GODARD D, ARCHAMBAULT P, AEBY-GAUTIER E, LAPASSET G. Precipitation sequences during quenching of the AA 7010 alloy [J]. *Acta Materialia*, 2002, 50(9): 2319–2329.
- [11] FINK W L, WILLEY L A. Quenching of 75S aluminium alloy [J]. *Transaction of American Institute of Mining, Metallurgical, and Petroleum Engineers*, 1948, 175: 414–427.
- [12] FLYNN R J, ROBINSON J S. The application of advances in quench factor analysis property prediction to the heat treatment of 7010 aluminium alloy [J]. *Journal of Materials Processing Technology*, 2004, 153–154: 674–680.
- [13] DOLAN G P, ROBINSON J S. Residual stress reduction in 7175-T73, 6061-T6 and 2017A-T4 aluminium alloys using quench factor analysis [J]. *Journal of Materials Processing Technology*, 2004, 153–154: 346–351.
- [14] ROBINSON J S, CUDD R L, TANNER D A. Quench sensitivity and tensile property inhomogeneity in 7010 forgings [J]. *Journal of Materials Processing Technology*, 2001, 119(1–3): 261–267.
- [15] LIU Sheng-dan, ZHANG Xin-ming, YOU Jiang-hai, HUANG Zhen-bao, ZHANG Chong, ZHANG Xiao-yan. TTP curve of 7055 aluminum alloy and its application [J]. *The Chinese Journal of Nonferrous Metals*, 2006, 16(12): 2034–2039. (in Chinese)
- [16] LIU Sheng-dan, ZHONG Qi-min, ZHANG Yong, LIU Wen-jun, ZHANG Xin-ming, DENG Yun-lai. Investigation of quench sensitivity of high strength Al–Zn–Mg–Cu alloys by time–temperature–properties diagrams [J]. *Materials and Design*, 2010, 31(6): 3116–3120.
- [17] SHANG Bao-chuan, YIN Zhi-min, WANG Gang, LIU Bo. Investigation of quench sensitivity and transformation kinetics during isothermal treatment in 6082 aluminum alloy [J]. *Materials and Design*, 2011, 32(7): 3818–3822.
- [18] STALEY J T. Quench factor analysis of aluminium alloys [J]. *Materials Science and Technology*, 1987, 3(11): 923–935.
- [19] PANIGRAHI S K, JAYAGANTHANA R, PANCHOLIA V, GPTA M. A DSC study on the precipitation kinetics of cryorolled Al 6063 alloy [J]. *Materials Chemistry and Physics*, 2010, 122(1): 188–193.
- [20] SATO Y S, KOKAWA H, ENOMOTO M, JOGAN S. Microstructural evolution of 6063 aluminum during friction-stir welding [J]. *Metallurgical and Materials Transactions A*, 1999, 30(9): 2429–2437.
- [21] BRATLAND D H, GRONG Ø, SHERCLIFF H, MYHR O R, TJØTTA S. Overview No. 124 Modelling of precipitation reactions in industrial processing [J]. *Acta Materialia*, 1997, 45(1): 1–22.
- [22] ZHANG D L, ZHENG L. The quench sensitivity of cast Al–7wt pct Si–0.4wt pct Mg alloy [J]. *Metallurgical and Materials Transactions A*, 1996, 27(12): 3983–3991.
- [23] DUTTA I, ALLEN S M. A calorimetric study of precipitation in commercial aluminium alloy 6061 [J]. *Journal of Materials Science Letters*, 1991, 10(6): 323–326.

6063 铝合金的 TTP 曲线与淬火敏感性

李红英^{1,2}, 曾翠婷¹, 韩茂盛¹, 刘蛟蛟¹, 鲁晓超¹

1. 中南大学 材料科学与工程学院, 长沙 410083;

2. 中南大学 有色金属材料科学与工程教育部重点实验室, 长沙 410083

摘要: 采用中断淬火技术测定了 6063 铝合金的时间–温度–性能(TTP)曲线, 透射电镜研究了 6063 铝合金的淬火敏感性。结果表明, 6063 铝合金的淬火敏感性低于 6061 和 6082 铝合金的, 合金的鼻尖温度为 360 °C, 淬火敏感区间为 300–410 °C。微观组织观察表明, 在敏感区间内, β -Mg₂Si 平衡相优先在(Al₃Fe₃Si₂)相上非均匀形核而析出, 且在 360 °C 鼻尖温度时的长大速度最快。平衡相的析出导致合金溶质原子的浓度下降, 减少了时效时的 β'' 强化相的数量, 降低了强化效果。因此, 对于 6063 铝合金大型材的淬火, 一方面, 在淬火敏感区间(410–300 °C)应加大冷却速率以抑制平衡相的析出, 从而获得较佳的时效强化效果; 另一方面, 适当减小从固溶温度到 410 °C 以及低于 300 °C 时的冷却速率, 从而减小淬火应力。

关键词: 6063 铝合金; 淬火敏感性; 硬度; 时间–温度–性能曲线; 强化相; 非均匀形核; 残余应力

(Edited by Hua YANG)